Earthquake Geotechnical Engineering for Protection and Development of Environment and Constructions – Silvestri & Moraci (Eds)
© 2019 Associazione Geotecnica Italiana, Rome, Italy, ISBN 978-0-367-14328-2

Plane strain modeling of basin-edge effects: Exploratory study in Wellington, New Zealand

C. McGann, C. de la Torre & B. Bradley
Department of Civil & Natural Resources Engineering, University of Canterbury, Christchurch, New Zealand

L. Wotherspoon
Department of Civil & Environmental Engineering, The University of Auckland, Auckland, New Zealand

ABSTRACT: Plane strain finite element modeling is undertaken to investigate factors contributing to basin-edge effects observed at sites in the Thorndon basin of Wellington, New Zealand in multiple seismic events. The models consider linear elastic soil and rock response to input SH-waves at the base. Depth-dependent shear wave velocities are assigned to the soil layers and various rock velocity structures are considered to evaluate their effect on the modeled surficial response at a reference site in the Thorndon basin. It is shown that these simple plane strain models are able to capture basin-edge-generated surface waves and basin reverberation effects. It is also shown that models with a horizontal impedance contrast across the Wellington Fault compare better in terms of spectral response and amplification at the reference site than models with a soil basin alone, and that conventional SH-1D site response models cannot capture the observed response across a range of periods.

1 INTRODUCTION

Sedimentary basins and valleys laterally confined by rock have long been known contribute to the amplification of seismic ground motions through several 2D and 3D effects commonly referred to as basin effects. These effects can be broadly separated into basin reverberation effects due to trapped wave energy repeatedly reflected between the free surface and the basin boundaries, and basin-edge effects due to resonance and constructive interference of basin-edge induced surface waves and vertically propagating SH-waves (Bard and Bouchon, 1980a, b).

Observed surficial ground motions at Wellington strong motion stations infer the presence of basin-edge effects at these sites in addition to significant local site effects, particularly for sites in the Thorndon basin in the 2016 Kaikōura event (Holden et al., 2013; Bradley et al., 2017, 2018). Numerical modeling of the Wellington region backs up these observations, with the 3D ground motion simulations of (Benites and Olsen, 2005) inferring similar response to that observed in previous events, and the plane strain models of Adams et al. (1999, 2003) demonstrating the development of basin-edge effects in the Lower Hutt Valley located about 8 km northwest of central Wellington.

In this paper, linear elastic plane strain wave propagation models are developed for a cross section through the Thorndon basin to further examine the mechanisms contributing to basin effects in Wellington. These models are analyzed for the 16 August 2013 M_w6.6 Lake Grassmere earthquake (Holden et al., 2013) to examine the role of the velocity structure of the rock underlying the soil basin through comparisons with the input rock motion, the observed surficial accelerations at a reference strong motion station within the basin, and corresponding SH1D site response analyses of the reference site. The plane of the model crosses the Wellington Fault Lensen (1958); Van Dissen and Berryman (1996), which has a near vertical dip and a strike direction nearly perpendicular to the model domain, and it is found that consideration

for a possible horizontal velocity contrast across this fault zone is a key factor in the development of basin-edge effects within the models.

2 MODEL DEVELOPMENT

All numerical models are developed and analyzed using the OpenSees finite element analysis platform (McKenna, 2011) and make use of stabilised single integration point quadrilateral elements (McGann et al., 2012) to model the soil and rock domain. In this exploratory study, only linear elastic constitutive response is considered, as the focus is on the wave propagation rather than details of the nonlinear soil behaviour.

2.1 *Basin model geometry*

The model domain for the current study is shown in Figure 1. This domain extends across the Wellington Fault through the Thorndon basin and Lambton Harbour, with a termination point at the southeastern end on the slopes of Mount Victoria near Oriental Bay. This domain is selected to support future numerical models of an instrumented structure in the Thorndon basin near a strong motion station that is taken as the reference site in the current study. It also allows for an assessment for the relative effects of the sedimentary soil basin and a potential rock basin formed by a velocity contrast between largely intact rock to the northwest of the Wellington Fault and the rock to the southeast which may be less stiff due to the presence of secondary faulting on this side of the main fault (Van Dissen and Berryman, 1996; GNS Science, 2009; Langridge et al., 2011).

The basin model is developed using digital elevation data to form the surface of the mesh, and the depth to bedrock contour map of Semmens et al. (2010) to establish the bounds of the soil basin. The Semmens et al. (2010) map provides bedrock depth over 10 m elevation intervals and is based on data from boreholes, test pits, site observations, and microtremor testing. The offshore regions of the Semmens et al. (2010) bedrock model are not well constrained by data, thus the basin model is supplemented by bathymetry data in this portion of the model domain. As discussed in subsequent sections, the soil layering and soil/rock shear wave velocities are also based in part on the surficial geologic mapping presented in Semmens et al. (2010).

Three mesh configurations are considered in order to gauge the effects of various modeling decisions and basin geometries. Figure 2 shows these these three configurations, which are referred to in all subsequent discussion as the base mesh, fault mesh, and deep mesh. Figure 2 also labels the various soil and rock layers considered and indicates the location of the reference site. To provide better resolution for the mesh within the basins, the true horizontal extents of the models are not shown in Figure 2, as these boundaries are extended well away from the soil basin to minimise boundary effects on the model response.

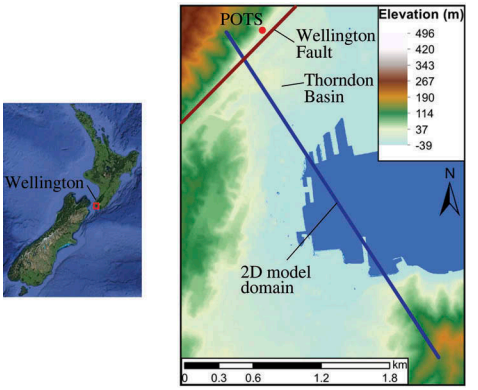

Figure 1. Map of Wellington area showing general area and orientation of plane strain basin model domain. The rock-sited POTS strong motion station and the location of the Wellington Fault are indicated for reference. Contours indicate surface elevation.

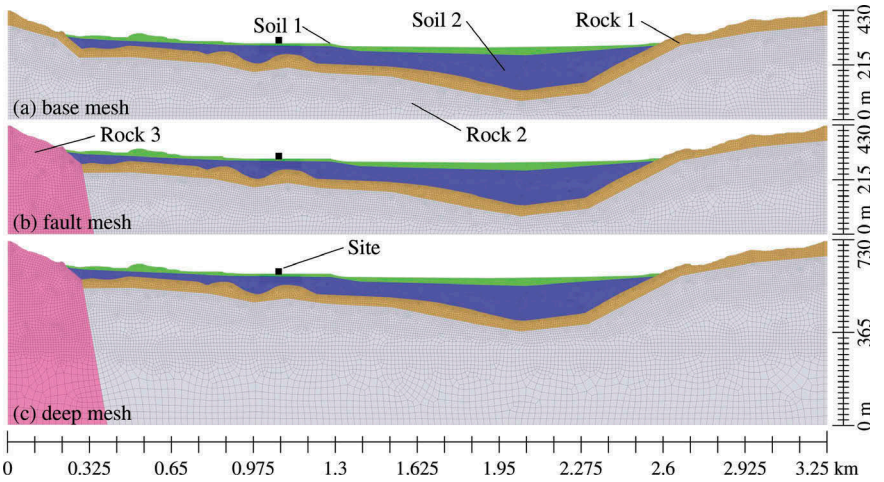

Figure 2. Three considered layouts for computational mesh. (a) Base mesh: soil basin only; (b) Fault mesh: horizontal impedance across Wellington Fault; (c) Deep mesh: deeper version of fault mesh.

2.2 *Soil properties*

The soil shear wave velocities are based on the results of surface wave V_s testing near the site in Wellington (Cox and Vantassel, 2018), CPT and SPT data obtained from the New Zealand Geotechnical Database near the site, and the range of values suggested by Semmens et al. (2010) for the various regional geologic units. Based on this available data, the soils in the basin are split into two general layers, a shallower layer with lower CPT/SPT resistances and V_s and a deeper denser layer with higher V_s (Soil 1 and Soil 2 layers in Figure 2, respectively). Depth-dependent shear wave velocity profiles are assigned to each of these layers as

$$V_s(z) = 160z^{0.25} \tag{1}$$

$$V_s(z) = 190z^{0.25} \tag{2}$$

where z is the depth in metres and V_s is in m/s. These distributions are selected to create a mild impedance contrast at the boundary of the two soils layers while keeping the velocities in the deeper portions of layer Soil 2 less than 700 m/s. Figure 3 shows the distribution of shear wave velocity within these two soils layers in the plane strain model. Both soil layers are assigned a Poisson's ratio of 0.3, and the densities are 1.7 and 1.8 Mg/m^3 for layers Soil 1 and 2, respectively.

2.3 *Rock properties*

Several rock velocity structures are considered for each of the mesh configurations in order to explore their impact on the basin-edge effects observed in the model. The eight distinct cases considered in the current study are summarised in Table 1. All cases consider the same soil properties, only the rock velocities are varied. The rock shear wave velocities assigned in the various cases are informed by Semmens et al. (2010), but the values used in the models are all assumed. The mass density values of all rock layers are assumed as $\rho = 2.6$ Mg/m^3 based on the work of Tenzer et al. (2010). Poisson's ratio values of 0.3 are also assumed for all rock layers.

The base mesh of Figure 2(a) considers only a soil basin underlain by rock and makes no consideration for any horizontal impedance contrasts within the rock layers due to regional secondary faulting. As shown in Table 1, two rock velocity structures are considered for the base mesh: a case where a band of 800 m/s weathered rock is underlain by very stiff 2000 m/s rock, and a case where the weathered rock is underlain by a rock layer with a 1000 m/s shear wave velocity.

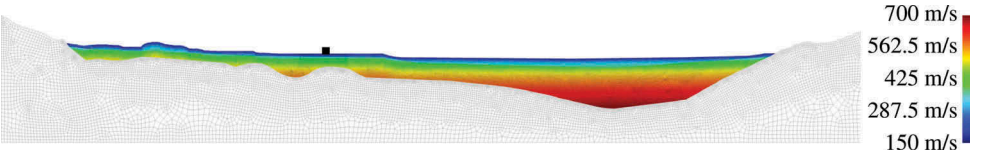

Figure 3. Depth-dependent shear wave velocity distribution in soil layers for all models.

Table 1. Rock velocity structure cases considered for three computational mesh configurations of Figure 2.

Mesh Configuration	V_s Rock 1 (m/s)	V_s Rock 2 (m/s)	V_s Rock 3 (m/s)
Base mesh	800	2000	–
	800	1000	–
Fault mesh	800	1250	2000
	800	1000	2000
	800	1500	2000
Deep mesh	800	1250	2000
	800	1000	2000
	800	1500	2000

The fault and deep mesh configurations of Figure 2(b) and (c) make simplified consideration for a horizontal impedance contrast across the Wellington fault, which as shown in Figure 1 passes through the modeled domain nearly perpendicular to the considered plane. The location of the fault in the plane strain models is clearly visible in Figure 2(b) and (c) as the boundary between layers Rock 2 and 3, where Rock 3 is the foot wall and Rock 2 forms the hanging wall. A dip angle of 80° is assigned to this fault boundary after Litchfield et al. (2012).

The cross-fault horizontal velocity contrast considered in these models is motivated primarily by the presence of second-order faults that bifurcate off of the main Wellington fault on the hanging wall side (Van Dissen and Berryman, 1996; GNS Science, 2009). Due to the presence of these secondary faults, it is likely that the rock on the hanging wall side is crushed and cracked, making it less stiff than the intact rock on the foot wall side. In addition, the rake angle for the fault is estimated at 15° (Litchfield et al., 2012), indicating a slight degree of normal fault movement may have occurred in previous ruptures, further contributing to greater stiffness on the foot wall side.

2.4 *Boundary and loading conditions*

The input ground motion is obtained from the rock-sited POTS strong motion station for the 16 August 2013 M_w6.6 Lake Grassmere event (see Figure 1 for location of POTS station relative to model domain). The recorded horizontal components recorded at POTS are rotated to align with the considered plane, and only the resulting in-plane component is applied to the model. This input motion has a PGA = 0.04 g, significant duration D_{5-95} = 15.1 s, predominant period of 0.42 s, and Arias intensity I_a = 0.0162 m/s. This motion is deconvolved and applied at the base of the model as input SH-waves using the method of Joyner and Chen (1975). In all cases, the properties of the underlying half-space are V_s = 2000 m/s and ρ = 2.6 Mg/m^3. Periodic boundary conditions are enforced at the horizontal extents of the models (not shown in Figure 2). Rayleigh damping is applied to the models with both mass and stiffness proportional terms such that the damping ratio is 5% at frequencies of 0.2 and 20 Hz. Vertical input motions are not considered.

2.5 *1D site response models for reference site*

One-dimensional (SH-1D) site response models are developed for the reference site (see Figure 2 for location) for each of the model configurations. These SH-1D models have identical layer,

mesh, and shear wave velocity distributions with depth as a vertical line drawn down through each model configuration below the reference site. The SH-1D models are analysed in OpenSees using a single column of quadrilateral elements with period boundary conditions and the same compliant base approach used in the 2D models. Comparisons between the SH-1D analyses and their corresponding 2D model allow for 1D and 2D wave propagation effects to be distinguished at the reference site. Note that three of the 2D models (one case for each 2D mesh) share the same 1D soil profile at the site (the second case for each mesh in Table 1).

3 OBSERVED AND SIMULATED RESULTS AT THE REFERENCE SITE

Figure 4 shows the response spectra at the model reference site for each of the eight cases summarised in Table 1 as compared to the input POTS motion and the observed surficial motion at the reference strong motion station. Model result are shown for the 2D basin model and corresponding SH-1D site response model for each case. As shown, the different mesh configurations and velocity structures in the 2D models all exhibit different levels of variability relative to the observed response and the corresponding SH-1D model. While there is certainly some variability across the different cases at lower periods, the range of periods between 1-2.5 seconds is of particular interest as this is where the basin effects are evident in the observed response spectrum.

Based on the results of Figure 4, it appears that the cases with a V_s of 1000 m/s in layer Rock 2 (Cases (b), (d), and (g) corresponding to Figure 4(b), (d), and (g), respectively) exhibit the most similarity to the observed response spectrum at the site both overall and in the 1-2.5 second period range. This is of particular interest as Cases (b) and (d) have identical 1D soil profiles below the reference site, and though Case (g) does not due to the deeper mesh, the 1D response spectrum in Figure 4(g) is nearly identical to that for Cases (b) and (d). Due to the identical/similar 1D response for these cases, any 1D and 2D effects can be clearly separated and any differences in the 2D model results can be attributed solely to differences in the 2D basin models.

Figure 5 directly compares the spectral amplification relative to the input POTS rock for these three 2D models relative to the amplification for the corresponding SH-1D model and the observed motion at the reference site. Comparison of the results for Cases (b) and (d) in Figure 5 is of particular interest, as the horizontal velocity contrast across the Wellington Fault is the only difference between these models, and therefore any differences in the response can be attributed to this velocity structure. There are several key differences. Firstly, the amplification at periods less than 0.1 seconds for the Base mesh is largely the same as the SH-1D analysis, while the Fault mesh produces amplifications more in line with observations at this range of periods. At longer periods, the Base mesh case tends to either over or under amplify relative to the Fault mesh. There are some clear shared features, for example the spike at 0.9 seconds and the dip just before 2 seconds, but in both cases the amplifications with the Fault mesh are closer to observations. The deep mesh shows much larger amplifications between 1.5-3 second periods, but it is unclear from just these results if this is due solely to the deeper profile of softer rock or some other effect.

The differences between these cases are explored further in Figure 6, which shows the vertical response spectra at the reference site. In Figure 6(a), the vertical acceleration for the POTS station is added to the recorded vertical accelerations from the models, while Figure 6(b) shows the vertical response spectra for the model results alone. Because vertical accelerations are not applied to the models, the vertical accelerations can only be caused by P-waves or Rayleigh waves generated within the models. None of the models come particularly close to reproducing the vertical response at the site, which is not surprising as the true vertical response is almost certainly influenced by 3D effects that cannot be captured in a 2D model. Of more interest are varying degrees of basin effects in the models as implied by the amplification at longer periods. As shown in Figure 6, the vertical response for Case (b) essentially matches the POTS response for periods >0.5 seconds, while the two cases with consideration for velocity variation across the fault show evidence of surface waves with characteristics more similar to what was observed at the site.

A final observation is supported by Figure 7, which shows the bias between the horizontal response spectra for the observed motion at the reference site and the various numerical

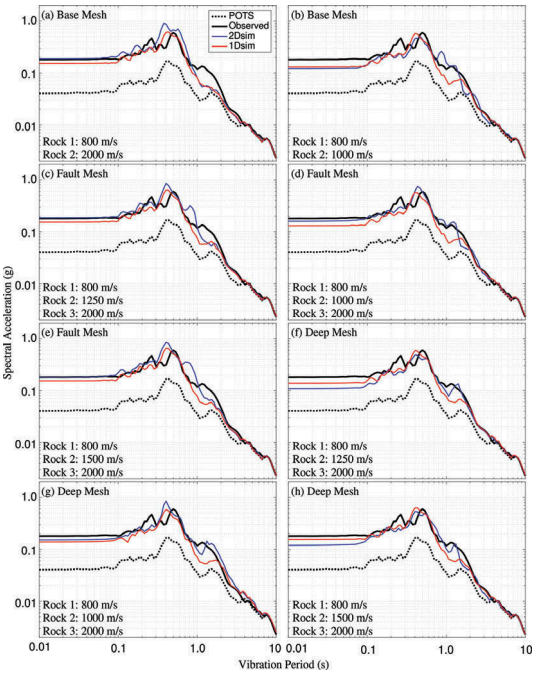

Figure 4. Horizontal response spectra from 1D and 2D models for all 8 model configurations compared to input bedrock motion (POTS) and the observed surficial motion at the reference site. Mesh case and rock shear wave velocities are indicated in each sub-figure.

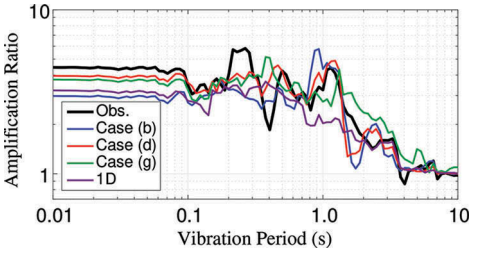

Figure 5. Spectral amplification of POTS motion for observed horizontal motion at reference site and all models with $V_s = 1000$ m/s for layer Rock 2.

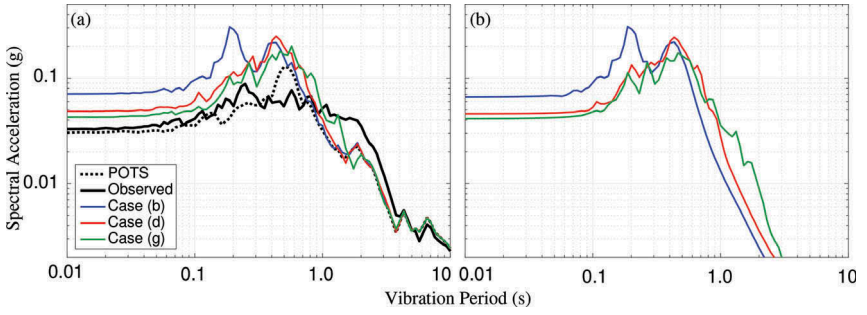

Figure 6. Vertical response spectra for analysis Cases (b), (d), and (g) from Figure 4. (a) Spectra for sum of model and POTS vertical accelerations; (b) Spectra for model vertical accelerations only.

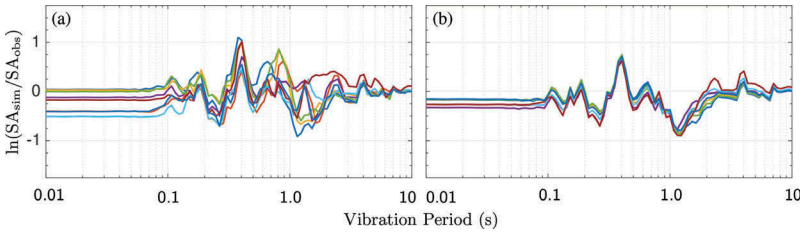

Figure 7. Bias with observed surface motion for all 8 model configurations. (a) 2D models; (b) 1D models.

models considered in this study. The 2D results shown in Figure 7(a) indicate far more variation across the various mesh configurations and velocity structures than is indicated in Figure 7(b) for the corresponding SH-1D models. This difference highlights the truly 2D (or even 3D) nature of the problem, as the SH-1D analyses have largely the same surficial motion despite differences in the 1D soil profile below the site. While the SH-1D models can match the observed response in the predominant period, they have an inherent limitation in matching the observed response across the full range of periods that can only be overcome through consideration of 2D or 3D analysis.

4 CONCLUSIONS

Linear elastic plane strain and SH-1D models were developed to examine the factors influencing basin effects for a reference site in the Thorndon Basin of Wellington, New Zealand. The plane strain models were used to assess the changes in the horizontal and vertical surficial motion recorded at the reference site for three mesh configurations and several velocity structures for the rock underlying the soil basin. Linear elastic models were chosen in order to place the emphasis of this study on wave propagation features rather than any near-surface nonlinear effects. The similarity of the simulations and observations shows that elastic wave propagation is a dominant factor in the surface acceleration at the reference site for Lake Grassmere earthquake. Due to the intensity of shaking observed, it is likely that nonlinear soil response occurred near the ground surface, and the absence of such response in the simulations may explain some of the remaining differences between the observed and simulated surficial response at the reference site.

The plane strain simulations indicate that a rock velocity structure where the shear wave velocity transitions from 800 m/s immediately below the soil to 1000 m/s and ultimately to 2000 m/s at depth produced results most similar to observations. It was also shown that models that considered a horizontal impedance contrast across the Wellington Fault, effectively creating a larger rock basin underlying the soil basin, compared better to the observations than models without this velocity structure, particularly for horizontal spectral accelerations in the 1-2.5 second period range and in terms of basin-generated surface waves. SH-1D models corresponding to each plane strain analysis case were unable to capture the observed response at a broad range of periods and these models were far less sensitive to changes in the rock velocity structure than the plane strain analyses. These shortcomings of the SH-1D analyses clearly demonstrated the need for 2D and 3D analyses in order to sufficiently capture the important aspects of site response in Wellington.

ACKNOWLEDGEMENTS

Elevation and bathymetry data was sourced from the LINZ Data Service (https://data.linz.govt.nz) and licensed by the Wellington Regional Council for re-use under the Creative Commons Attribution 4.0 International license. Seismograms were obtained from the New Zealand Strong Motion Database (Van Houtte et al., 2017). This work was supported by QuakeCoRE, a New Zealand Tertiary Education Commission-funded Centre. This is QuakeCoRE publication number 0345.

REFERENCES

Adams, B.M., Davis, R., Berrill, J., & Taber, J. 1999. *Two-dimensional site effects in Wellington and the Hutt Valley - Similarities to Kobe*. University of Canterbury Research Report No. 99–103, Department of Civil Engineering, University of Canterbury.

Adams, B.M., Osborne, N.M., & Taber, J.J. 2003. The basin-edge effect from weak ground motions across the fault-bounded edge of the Lower Hutt Valley, New Zealand. *Bulletin of the Seismological Society of America* 93(6): 2703–2716.

Bard, P.Y. & Bouchon, M. 1980a. Seismic response of sediment filled valleys Part 1: The case of incident SH waves. *Bulletin of the Seismological Society of America* 70(4): 1263–1286.

Bard, P.Y. & Bouchon, M. 1980b. Seismic response of sediment filled valleys Part 2: The case of incident P and SV waves. *Bulletin of the Seismological Society of America* 70(4): 1921–1941.

Benites, R. & Olsen, K.B. 2005. Modeling strong ground motion in the Wellington metropolitan area, New Zealand. *Bulletin of the Seismological Society of America* 95(6): 2180–2196.

Bradley, B.A., Wotherspoon, L.M., & Kaiser, A.E. 2017. Ground motion and site effect observations in the Wellington region from the Kaikura, New Zealand earthquake. *Bulletin of the New Zealand Society for Earthquake Engineering* 50(2): 94–105.

Bradley, B.A., Wotherspoon, L.M., Kaiser, A.E., Cox, B.R., & Jeong, S. 2018. Influence of site effects on observed ground motions in the Wellington region from the Kaikura, New Zealand, earthquake. *Bulletin of the Seismological Society of America* 108(3B): 1722–1735.

Cox, B.R. and Vantassel, J. 2018. *Dynamic Characterization of Wellington, New Zealand*. DesignSafe-CI [publisher], Dataset, doi: 10.17603/DS24M6J.

GNS Science 2009. New research shows lower threat from Wellington fault [online news release]. https://www.gns.cri.nz/Home/News-and-Events/Media-Releases/Lower-threat-from-Wellington-fault, Published online 18/09/2009; Accessed 11/12/2018.

Holden, C., Kaiser, A., Van Dissen, R., & Jury, R. 2013. Sources, ground motion and structural response characteristics in wellington of the 2013 cook strait earthquakes. *Bulletin of the New Zealand Society for Earthquake Engineering* 46(4): 188–195.

Joyner, W.B. & Chen, A.T.F. 1975. Calculation of nonlinear ground response in earthquakes. *Bulletin of the Seismological Society of America* 65(5): 1315–1336.

Langridge, R., Van Dissen, R.J., Rhoades, D., Villamor, P., Little, T., Litchfield, N., Clark, K., & Clark, D. 2011. Five thousand years of surface ruptures on the Wellington fault, New Zealand: Implications for recurrence and fault segmentation. *Bulletin of the Seismological Society of America* 101(5): 2088–2107.

Lensen, G.J. 1958. The Wellington fault from Cook Strait to Manawatu Gorge. *New Zealand Journal of Geology and Geophysics* 1(1): 178–196.

Litchfield, N.J., Van Dissen, R., Sutherland, R., Barnes, P.M., Cox, S.C., Norris, R., Beavan, R.J., Langridge, R., Villamor, P., Berryman, K., Stirling, M., Nicol, A., Nodder, S., Larmarche, G., Barrell, D.J.A., Pettinga, J.R., Little, T., Pondard, N., Mountjoy, J., & Clark, K. 2012. *A model of active faulting in New Zealand: fault zone parameter descriptions*. GNS Science Report 2012/19, GNS, Lower Hutt, New Zealand.

McGann, C.R., Arduino, P., & Mackenzie-Helnwein, P. 2012. Stabilized single-point 4-node quadrilateral element for dynamic analysis of fluid saturated porous media. *Acta Geotechnica* 7(4): 297–311.

McKenna, F. 2011. Opensees: A framework for earthquake engineering simulation. *Computing in Science and Engineering* 13(4): 58–66.

New Zealand Geotechnical Database 2018. https://www.nzgd.org.nz. Accessed 20/07/2018.

Semmens, S., Perrin, N.D., & Dellow, G.D. 2010. *It's Our Fault - Geological and Geotechnical Characterisation of the Wellington Central Business District*. GNS Science Consultancy Report 2010/176, GNS, Lower Hutt, New Zealand.

Tenzer, R., Sirguey, P., Rattenbury, M., & Nicolson, J. 2010. A digital rock density map of New Zealand. *Computers & Geosciences* 37(8): 1181–1191.

Van Dissen, R.J. & Berryman, K.R. 1996. Surface rupture earthquakes over the last 1000 years in the Wellington region, New Zealand, and implications for ground shaking hazard. *Journal of Geophysical Research* 101(B3): 5999–6019.

Van Houtte, C., Bannister, S., Holden, C., Bourguignon, S., & McVerry, G. 2017. The New Zealand Strong Motion Database. *Bulletin of the New Zealand Society for Earthquake Engineering* 50(1): 1–20.